Impact of the photoelectric threshold sensitivity on the work function determination: revealing ultra-low work functions of caesiated surfaces

Adrian Heiler, Roland Friedl, Ursel Fantz

Angaben zur Veröffentlichung / Publication details:

Heiler, Adrian, Roland Friedl, and Ursel Fantz. 2022. "Impact of the photoelectric threshold sensitivity on the work function determination: revealing ultra-low work functions of caesiated surfaces." *AIP Advances* 12 (3): 035339. https://doi.org/10.1063/5.0078380.

AIP Advances

Impact of the photoelectric threshold sensitivity on the work function determination—Revealing ultra-low work functions of caesiated surfaces

Cite as: AIP Advances 12, 035339 (2022); https://doi.org/10.1063/5.0078380
Submitted: 31 January 2022 • Accepted: 25 February 2022 • Published Online: 18 March 2022

A. Heiler, R. Friedl and U. Fantz

Impact of the photoelectric threshold sensitivity on the work function determination—Revealing ultra-low work functions of caesiated surfaces

Cite as: AIP Advances 12, 035339 (2022); doi: 10.1063/5.0078380
Submitted: 31 January 2022 • Accepted: 25 February 2022 •
Published Online: 18 March 2022

A. Heiler,[1,2,a] R. Friedl,[2] and U. Fantz[1,2]

AFFILIATIONS

[1] Max-Planck-Institut für Plasmaphysik, Boltzmannstrasse 2, D-85748 Garching, Germany
[2] AG Experimentelle Plasmaphysik, Universität Augsburg, D-86135 Augsburg, Germany

[a] Author to whom correspondence should be addressed: adrian.heiler@ipp.mpg.de

ABSTRACT

The exploitation of the photoelectric effect is a prominent method for the *in situ* measurement of the absolute work function of a surface. In the case of metallic surfaces, the Fowler theory is routinely applied for fitting or extrapolating the measured photoelectric yield data to determine the work function value. However, for the reliable application of the Fowler method, attention must be paid to the experimental sensitivity to the photoelectric behavior close to the threshold, which is mainly determined by the signal-to-noise ratio for photocurrent detection and the available photon energies used for irradiation. This is illustrated by means of applying a photoelectric work function measurement system during a Cs coating process of a metal surface, where insufficiently low photon energies or an unfavorable noise level can lead to a severe overestimation of the work function of the order of 1 eV. By a sufficient enhancement of the photoelectric sensitivity, it is now unveiled that ultra-low surface work functions of 1.25 ± 0.10 eV can be generated via caesiation of metallic surfaces (here molybdenum and stainless steel) under vacuum conditions of 10^{-6}–10^{-5} mbar, which is most probably the result of the formation of an oxidized Cs adlayer.

I. INTRODUCTION

A standard experimental procedure for the *in situ* determination of the absolute electronic work function is the measurement of photoelectric currents extracted by electromagnetic irradiation with varying photon energies. Due to a finite detection limit in the experiment and often limited available photon energies (e.g., restricted lower limit or energy resolution), the evaluation of the work function is then typically performed by fitting or extrapolating the measured photoelectric yield curve, for which the application of the semi-classical Fowler theory[1] for metal–vacuum interfaces is common practice.[2–10] Compared to the methods based on thermionic emission, field electron emission, or a contact potential electrode, the photoelectric method has the advantage that high temperatures, high electric fields, and contact with other materials are not required.[11,12]

Although photoelectric yield curves can, in principle, easily be determined, it requires some—often underestimated—effort to deduce reliable work function values from it. First, the energy resolution of the irradiated light must be appropriate, i.e., a sufficient amount of photon energies with a narrow spectral bandwidth or a continuously tunable light source is required, and second, a sufficient signal-to-noise ratio (SNR) for the photocurrent detection must be provided. The SNR depends on the power irradiation onto the surface (for a fixed illumination area) and on the level of the dark current, i.e., the current that is measured without irradiation. The dark current represents the noise level for the photoelectric measurement and is determined by the quality of the electric circuit, external noise sources, the conditions in the vacuum system, etc. The SNR is especially decisive in the vicinity of the photoelectric threshold, where the photocurrents generally decrease rapidly when the photon energies $h\nu$ approach the work function χ. In this region, i.e., $h\nu \gtrapprox \chi$, the photocurrents must be tracked very carefully so that the Fowler method can be applied reliably.

The present paper is a continuation of the work described in Ref. 13, where the importance of the threshold determination is already discussed as decisive for the accuracy of determined work function values via the Fowler method and where the work function dynamics of a metal surface that is subject to Cs adsorption is investigated. In this work, the same adsorption system is analyzed, but the irradiation frequencies of the work function measurement setup are extended to photon energies <3 eV and the SNR is substantially enhanced. By these improvements, the impact of an insufficient experimental photoelectric sensitivity is now impressively and reproducibly shown in a much wider range of work function values. Moreover, it is now demonstrated that ultra-low surface work functions can be generated by the caesiation of metal substrates under vacuum conditions of some 10^{-6} mbar.

II. PHOTOELECTRIC EMISSION FROM METALS INTO VACUUM

The photoelectric threshold is defined as the minimum photon energy required to extract an electron from the interior of a solid state into vacuum. For metals at absolute zero temperature, the photoelectric threshold is equal to the energy difference between the Fermi level and the vacuum level and, thus, to the electronic work function χ.[14] For temperatures $T > 0$ K, a portion of the electrons at the Fermi edge is elevated to energies beyond the Fermi level due to thermal excitations, which is illustrated in Fig. 1 by plotting the product of the 3D density of states of a Fermi gas and the Fermi–Dirac distribution as a function of the electron energy ε_e for $T = 300$ and 1000 K, respectively. The chemical potential is set to a good approximation equal to the Fermi energy ε_F (here, 4 eV).

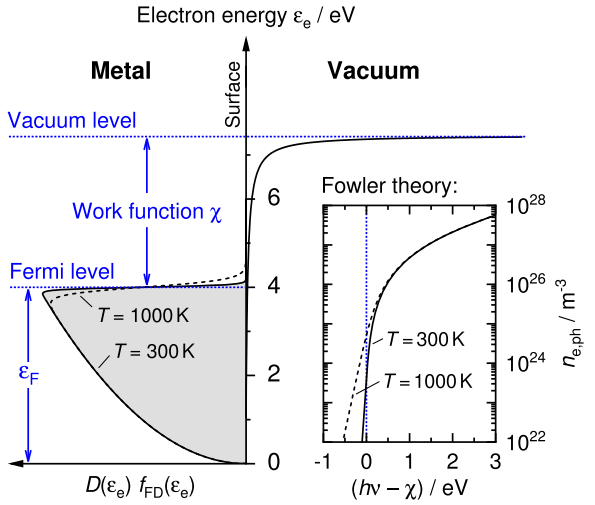

FIG. 1. Illustration of the energy diagram of a metal–vacuum interface. For $T > 0$ K, the occupied electronic states in the metal [gray shaded area, calculated from the 3D density of states $D(\varepsilon_e)$ of a Fermi gas] are thermally smeared at the Fermi level according to the Fermi–Dirac distribution $f_{FD}(\varepsilon_e)$. The surface potential barrier is represented by an image potential of the released electron. The inset shows the density of photoelectrically releasable electrons as a function of the energy difference between the irradiated photon energy and the work function according to the Fowler theory [Eq. (2)] for $T = 300$ and 1000 K, respectively ($\varepsilon_F = 4$ eV).

The energy dispersion is of the order of $k_B T$, which is 0.026 eV at 300 K and 0.086 eV at 1000 K, with k_B denoting the Boltzmann constant. Since all the measurements in this work are performed at about room temperature, the energy smearing at the Fermi level is, hence, very weak and the photoelectric threshold of the metal can be set in a good approximation equal to the work function.

A. Fowler theory

One of the most prominent theories for photoelectric electron emission at metal–vacuum interfaces is the Fowler theory. On the basis of Sommerfeld's theory of free electron gas, Fowler assumed that the photoelectric current per unit incident light intensity, $I_{ph,u}$, is to a good approximation proportional to the density $n_{e,ph}$ of electrons in the metal whose kinetic energy component normal to the surface exceeds the surface potential barrier after the augmentation by $h\nu$ due to photon absorption.[1] Accordingly, the electron density determining the photoelectric current is calculated as

$$n_{e,ph} = 2\left(\frac{m}{h}\right)^3 \int_{u'}^{\infty} du \int_0^{2\pi} d\varphi \int_0^{\infty} d\rho \frac{\rho}{\exp\left(\frac{\frac{1}{2}m(u^2+\rho^2)-\varepsilon_F}{k_B T}\right)+1}, \quad (1)$$

where u is the velocity component of the electrons normal to the surface and $u' = \sqrt{2(\varepsilon_F + \chi - h\nu)/m}$ is the minimum velocity component normal to the surface such that after the addition of $h\nu$, the electron can leave the solid state. m and T denote the free electron mass and the absolute temperature of the irradiated surface, respectively. By solving the ρ- and φ-integrals and by using the substitution variable $y = 1/2mu^2/(k_B T)$, Eq. (1) can be written as[1]

$$n_{e,ph} = \tilde{C} T^{3/2} \int_0^{\infty} \frac{\ln[1+\exp(-y+\kappa)]}{\sqrt{y-\kappa+\varepsilon_F/(k_B T)}} dy \quad (2)$$

with $\kappa := (h\nu - \chi)/(k_B T)$ and the constant $\tilde{C} := 2\sqrt{2}\pi(k_B m)^{3/2}h^{-3} \approx 1.36 \times 10^{21}$ m^{-3} K$^{-3/2}$.

In the inset of Fig. 1, the evolution of $n_{e,ph}$ according to Eq. (2) is demonstrated as a function of $h\nu - \chi$ for $T = 300$ and 1000 K, respectively. As can be seen, the number of photoelectrically releasable electrons decreases strongly for $h\nu \to \chi$ with $h\nu > \chi$, and consequently, a high sensitivity is required in the experiment to detect photocurrents as close as possible to the work function. For $h\nu \le \chi$, $n_{e,ph}$ continues to drop steeply: while the decrease at 1000 K is two orders of magnitude within 0.4 eV, at 300 K, it is already within 0.1 eV.

Since Eq. (2) is not well suited for the experimental application due to the typically unknown Fermi energy (in particular in the context of adsorption processes), approximations have to be made. If only photon energies close to the work function are considered, i.e., $h\nu \approx \chi$, Eq. (2) can be simplified to[1]

$$n_{e,ph}^{1st\ approx.} = \frac{\tilde{C} T^{3/2}}{\sqrt{\varepsilon_F/(k_B T) - \kappa}} f(\kappa) \quad (3)$$

and further to[1]

$$n_{e,ph}^{2nd\ approx.} = C T^2 f(\kappa), \quad (4)$$

with the constant $C := \check{C} k_B^{1/2} \varepsilon_F^{-1/2}$ and f denoting the temperature dependent function

$$f(\kappa) := \int_0^\infty \ln[1 + \exp(-y + \kappa)]\mathrm{d}y \tag{5}$$

$$= \begin{cases} \sum_{n=1}^{\infty} (-1)^{n+1} \exp(n\kappa)/n^2, & \kappa \le 0, \\ \pi^2/6 + \kappa^2/2 + \sum_{n=1}^{\infty} (-1)^n \exp(-n\kappa)/n^2, & \kappa \ge 0. \end{cases} \tag{6}$$

The predicted progression $I_{ph,u} \propto n_{e,ph}^{2nd\ approx.}$ has proven excellent experimental agreement for irradiation frequencies near the photoelectric threshold,[1,15,16] and thus, it is routinely applied as the basis for photoelectric work function evaluations.[6,8,10,17] An even more succinct simplification is obtained for the temperature limit $T \to 0$ K,[1]

$$n_{e,ph}^{T\to 0} \begin{cases} = 0, & h\nu \le \chi, \\ \propto (h\nu - \chi)^2, & h\nu > \chi, \end{cases} \tag{7}$$

whose application is also common practice.[2–5,7,9] Akbi *et al.*[10] pointed out, however, that the $T = 0$ K approximation may introduce errors of the order of $k_B T$, and thus, Eq. (4) should be preferred (as long as ε_F is not known).

B. Experimental realization

In order to track the progression of the frequency dependent photoelectric yield experimentally, a tunable light source with a narrow spectral bandwidth is required. Since the application of a laser with a continuously variable frequency is expensive, a set of several discrete photon energies can be used instead, provided by lasers or light-emitting diodes, for instance. In this work, the discrete photon energies are provided conveniently by the broadband emission of a high pressure mercury lamp (Osram HBO 100W/2) in combination with a set of interference filters (10 nm nominal FWHM), as done in Ref. 13. Different from the setup used in Ref. 13, however, the interference filter set has been extended: 11 filters with central transmission wavelengths between 430 and 852 nm have been added to the former nine filters in the range of 239–405 nm in order to provide lower irradiation frequencies. The interference filters are mounted in a motorized filter wheel in front of the lamp, which can house six filters. The setup is installed at the laboratory experiment ACCesS,[18] and as illustrated in Fig. 2, the transmitted light is collimated via two quartz lenses and is directed through a quartz viewport into a cylindrical stainless steel vacuum chamber. In the chamber, an electrically insulated sample holder is attached to the bottom plate, and the surface temperature of installed samples at the sample holder is measured with a K-type thermocouple. The illumination spot on the sample surface has a diameter of about 15 mm. The emission spectrum of the mercury lamp together with the respective transmitted spectra through the applied filters is recorded with a spectrometer and is depicted in Fig. 2(a). The corresponding transmitted mean photon energies ε_{ph} through the filters are determined after calibrating the transmission spectra and yield ε_{ph} = 5.04–3.05 eV for the formerly used restricted filter set and ε_{ph} = 5.04–1.45 eV for the extended filter set into the near-infrared (energy resolution mostly in the range of 0.1–0.3 eV).

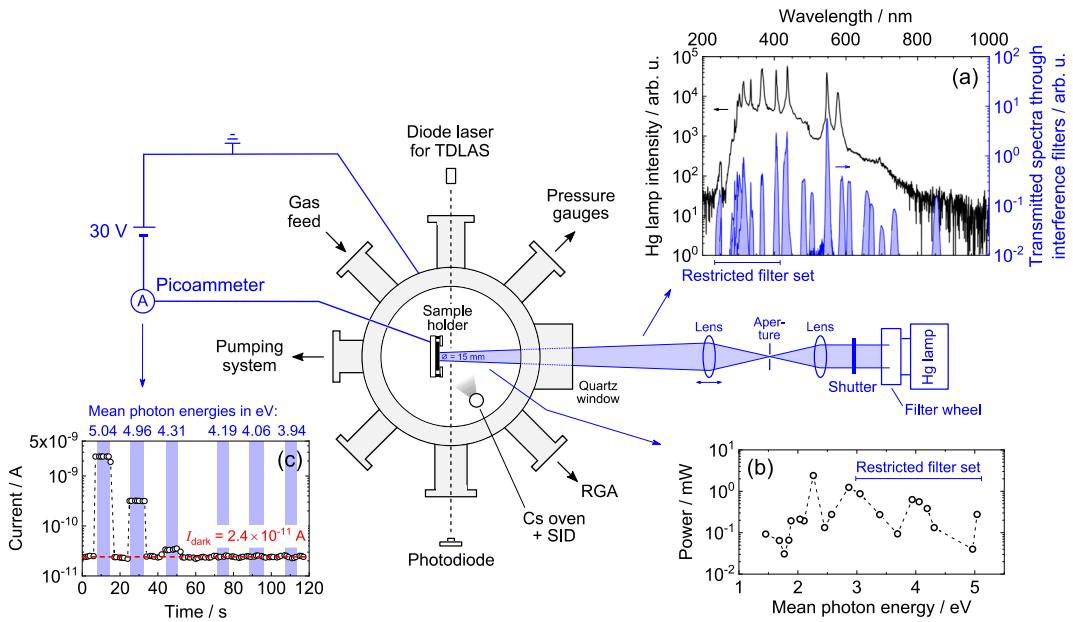

FIG. 2. Sketch of the experimental setup ACCesS where the photoelectric work function measurements are conducted. The emission spectrum of the mercury lamp together with the transmitted spectra through the interference filters used for the work function diagnostic is depicted in (a), and the energy resolved irradiation power onto the sample surface is plotted in (b). In (c), an exemplary photocurrent monitoring for photon energies in the range of 5.04–3.94 eV is shown, with the state of the shutter being open indicated in blue.

The irradiation power onto the sample surface is measured with a radiant powermeter (Newport model 818-UV/DB) and is shown in Fig. 2(b).

The photoemitted electrons are drawn to the grounded vessel walls by means of an electric field above space charge limitation, which is done by applying a bias of −30 V to the sample holder and surface. The execution of the work function measurement is realized by an automated data acquisition and evaluation procedure by using a Keithley 6487 picoammeter and a LabVIEW program: while the current is continuously recorded, a shutter opens in the optical path for each of the six filters in the filter wheel for a period of typically a few seconds, as demonstrated in Fig. 2(c). The respective absolute photocurrents $I_{\mathrm{ph}}(\varepsilon_{\mathrm{ph}})$ are subsequently calculated by averaging the current measured during the time the shutter is open and subtracting the dark current I_{dark}, which is, in turn, determined by averaging the currents measured when the shutter is closed before and after the respective irradiation phase. With the present setup, the SNR, i.e., the ratio of the photocurrent to the dark current, must be $\gtrsim 0.03$ so that the photocurrent can be distinguished from the dark current. The dark current is typically of the order of 10^{-11}–10^{-10} A, and thus, photocurrents down to the pA range can be detected. In case the dark current is highly dynamic during one measurement (factors influencing the dark current are discussed in Sec. III B), a polynomial interpolation and subsequent subtraction of the dark current is preferred. Finally, the absolute photocurrents are divided by the square of the measured surface temperature and the filter dependent relative intensities $F(\varepsilon_{\mathrm{ph}})$ of the irradiated light [calculated from Fig. 2(b) after the conversion of the irradiation power from mW to photons/s], and the logarithm of $I_{\mathrm{ph}}/(FT^2)$ is plotted as a function of the photon energy, which according to Eq. (4) is fitted via

$$\ln\left[\frac{I_{\mathrm{ph}}(\varepsilon_{\mathrm{ph}})}{F(\varepsilon_{\mathrm{ph}})T^2}\right] = A + \ln\left[f\left(\frac{\varepsilon_{\mathrm{ph}}-\chi}{k_{\mathrm{B}}T}\right)\right], \tag{8}$$

with the work function χ and the constant A being fit parameters. The representation of the photocurrents according to Eq. (8) corresponds to a (classical) Fowler plot,[1] and the respective work function evaluation is known as the Fowler method of isothermal curves. In accordance with the considerations given in Ref. 13, the six interference filters that are inserted into the filter wheel are chosen after identifying the filter with the lowest photon energy with which a photoelectric response is still obtained in order to meet the condition $h\nu \gtrapprox \chi$. Since one measurement takes typically about 2 min [see Fig. 2(c)], the identification of the appropriate filter set can last several minutes. This is relevant for dynamic surface work functions as in the case of the conducted caesiation processes in this work, where changes on the minute scale can occur (see discussion in Sec. IV).

The vacuum vessel with a diameter of 15 cm and a height of 10 cm is evacuated by using a turbomolecular and roughing pump and provides vacuum conditions of 10^{-6}–10^{-5} mbar (unbaked, limited by Viton O-ring seals). The residual gas pressure is measured with a cold cathode gauge, and its composition is monitored with a differentially pumped residual gas analyzer (RGA, not yet calibrated for absolute partial pressures). The alkali metal Cs can be evaporated into the experiment by means of a Cs oven, which is attached to the bottom plate of the vacuum vessel and which was designed and manufactured at IPP Garching (Germany).[19] The Cs oven contains a liquid Cs reservoir (1 g Cs ampoule), which can be heated in a controlled manner to finely adjust the Cs evaporation rate. The nozzle of the oven is directed toward the sample holder so that installed metal samples can be coated via Cs adsorption, which is well known to strongly reduce the surface work function due to the high electropositivity of Cs.[20,21] To monitor the Cs evaporation rate, a surface ionization detector (SID) is located a few millimeters behind the oven nozzle. The SID consists of two tungsten filaments (300 μm diameter) that are biased against each other with ≈60 V and are ohmically heated by passing a current of 2–3 A through each of them. Cs atoms are ionized when they approach the first hot tungsten filament and are subsequently accelerated and collected onto the second filament. The resulting current is proportional to the impinging flux of Cs atoms onto the first filament and is thus a measure of the Cs outflow from the oven nozzle.[22] Moreover, the neutral Cs density n_{Cs} in the chamber is measured along the 15 cm line-of-sight parallel to and close to the sample surface by means of a tunable diode laser absorption spectroscopy (TDLAS) system (detection limit $\approx 2 \times 10^{13}$ m^{-3}).[23]

The ACCesS experiment is mainly dedicated to study the work function performance and H^- yield of caesiated metallic surfaces in a low pressure low temperature hydrogen plasma environment.[17,24,25] This is done in view of negative hydrogen ion sources that rely on the production of negative ions on caesiated converter surfaces,[26] which are used for fusion and accelerator applications for instance.[27] The discharges at ACCesS are generated via inductive radio frequency (RF) coupling by using a planar solenoid on top of the vessel and an RF generator operating at 27.12 MHz and with 600 W maximum output power. Gas feeding is done by using calibrated mass flow controllers.

III. DECISIVE PARAMETERS FOR THE PHOTOELECTRIC WORK FUNCTION EVALUATION

It is well known that the work function of a surface strongly depends on its physical and chemical conditions, such as surface roughness, crystallographic orientation, the presence of contaminants, and surface adsorbates. The analysis of the photoelectric work function evaluation in this work is performed with a polycrystalline Mo substrate (3 μm Mo coating on a 30 × 30 × 5 mm^3 Cu sample) in a vacuum environment of about 5×10^{-6} mbar at room temperature. The Mo substrate, whose work function is >4 eV (experimentally measured after hydrogen plasma cleaning, see Sec. IV, and in accordance with literature values[28–30]) is exposed to Cs vapor in order to provide a strongly varying work function upon surface adsorption. Since the nozzle of the Cs oven in the vacuum chamber is set to a temperature of ≈550 K to avoid Cs sticking, the temperature of the Mo substrate increases slightly by a few degrees over a period of several hours due to thermal radiation (~ 1 K/h). It has to be noted that the Mo substrate used in this section is pre-caesiated from an earlier campaign, leading to an already reduced work function <4 eV.

A. Lower limit of available photon energy

In Fig. 3(a), measured surface work functions during a re-caesiation process of the Mo substrate are shown, where the neutral Cs density in the gas phase is continuously monitored via laser

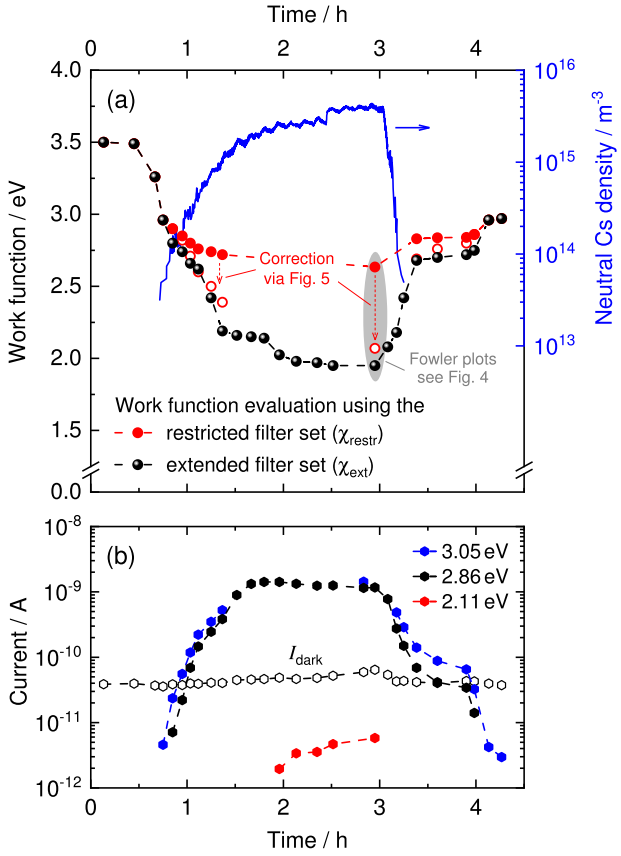

FIG. 3. Caesiation of a degraded pre-caesiated Mo surface at about room temperature. In (a), the measured neutral Cs density is plotted together with the work function evaluated by using the restricted and the extended filter set. The correction method after Ref. 13 is applied to the work functions determined with the restricted filter set (open symbols; details are illustrated in Fig. 5). In (b), measured photoelectric currents for some of the irradiated photon energies and the dark current are shown.

absorption. Photocurrents obtained with some of the irradiated photon energies together with the dark current are plotted in Fig. 3(b). The initial work function of the degraded Cs adlayer is 3.5 eV. By ramping up the Cs evaporation rate, the photocurrents significantly increase and the surface work function is reduced. The evaluation of the measured photocurrents via a Fowler plot [Eq. (8)] using the extended interference filter set (applied filters in the filter wheel are appropriately adjusted) reveals a drastic reduction of the surface work function to slightly below 2 eV at a reached Cs density of 2.6×10^{15} m^{-3} ($t \approx 2.1$ h). Under the assumption of an isotropic thermal distribution of Cs within the vessel, the corresponding Cs flux onto the surface can be calculated via $\Gamma_{Cs} = n_{Cs}\langle v_{Cs}\rangle/4 = 1.6 \times 10^{17}$ m^{-2} s^{-1}, with $\langle v_{Cs}\rangle$ being the mean thermal velocity of the Cs atoms (temperature ~ 400 K, obtained by the TDLAS line profile). Ripples in the measured Cs density are a characteristic of the Cs oven used and result from a slightly oscillating temperature regulation (≈ ±5 K) of some of the oven's inner surfaces.

By keeping the Cs density above 10^{15} m^{-3} for ≈1 h, the surface work function of slightly below 2 eV is maintained. The generation of such a low work function (here in the range of bulk Cs[29,30]) is remarkable due to the moderate vacuum level in the experimental chamber and is further discussed in Sec. IV. As soon as the Cs evaporation is reduced and finally shut down ($t > 3$ h), the photoelectric yields decrease rapidly and the photoelectric threshold and, thus, the work function increase strongly.

As can be seen in Fig. 3(a), the work functions χ_{restr} that are evaluated in case the restricted filter set (minimum photon energy = 3.05 eV; see Fig. 2) is used are higher compared to the values $\chi_{ext} \lesssim 2.8$ eV that are evaluated with the extended filter set. The deviation becomes larger as χ_{ext} becomes smaller, and when $\chi_{ext} \sim 2$ eV, a 0.7 eV larger value is evaluated with the restricted filter set. The reason behind this is demonstrated in the following: an exemplary Fowler plot created from the measured photocurrents at $t \approx 3.0$ h for photon energies in the range of $\varepsilon_{ph} = 2.04$–5.04 eV is shown in Fig. 4(a), with 2.04 eV being the lowest photon energy with which

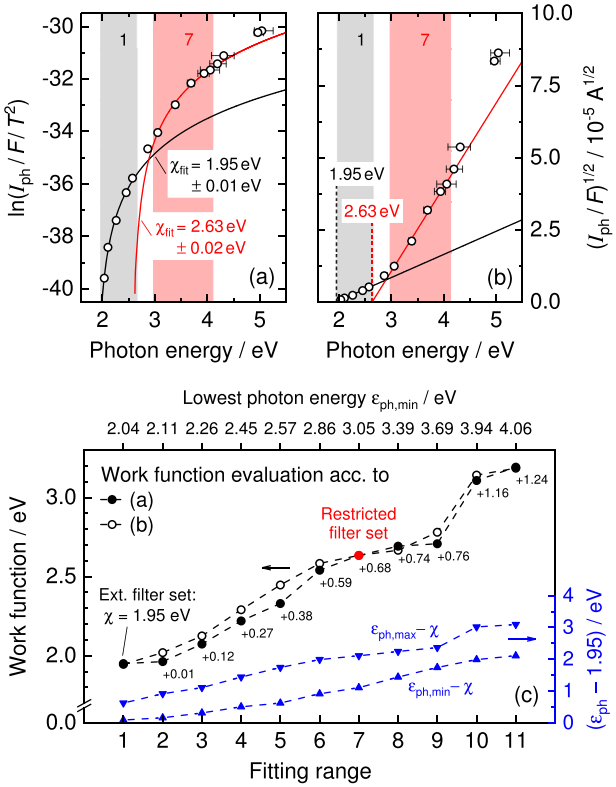

FIG. 4. Evaluation of the work function based on the photoelectric yield curve that is measured during the re-caesiation process shown in Fig. 3 at $t \approx 3.0$ h (substrate temperature = 306 K). The evaluation is demonstrated via a Fowler plot in (a) and via the Fowler $T = 0$ K approximation in (b) for the case the extended filter set is used (fitting range 1: gray shaded area) and for the case that photon energies <3 eV are not available (restricted filter set, fitting range 7: red shaded area). In (c), the determined work functions are plotted as a function of the method and the used fitting range comprising each time five consecutive photocurrents. The difference of the work functions determined via the Fowler plot to the determined threshold of 1.95 eV is labeled. The distances of the lowest and highest photon energies of each fitting range ($\varepsilon_{ph,min}$ and $\varepsilon_{ph,max}$) to the threshold of 1.95 eV are additionally plotted.

photoelectric response is detected (next lower photon energy without photoelectric signal is 1.88 eV). The x-error bars result from the transmitted wavelength ranges of the interference filters with a cutoff at 5% of the normalized transmitted spectrum. A fit of the five photocurrents obtained for the lowest photon energies, i.e., ε_{ph} = 2.04–2.57 eV (gray shaded area), yields χ_{fit} = 1.95 ± 0.01 eV, with ±0.01 eV being the standard error of the performed fit. The fitted function is extrapolated to $\varepsilon_{ph} \sim 5$ eV, which shows that the photocurrents for photon energies far above the evaluated threshold of 1.95 eV are underestimated by the Fowler theory, with the deviation becoming larger the further the photon energies are above the threshold. Consequently, a shift of the fitting range consisting of five consecutive photocurrents ($\varepsilon_{ph,max} - \varepsilon_{ph,min} \lesssim 1$ eV) to higher $\varepsilon_{ph,min}$ leads to a gradually increasing steepness of the Fowler fit and, thus, to the evaluation of increasing work function values. The dependence of the evaluated work function as a function of the fitting range is shown in Fig. 4(c), where the distances of $\varepsilon_{ph,min}$ and $\varepsilon_{ph,max}$ of each fitting range to the threshold of χ = 1.95 eV (which is expected to be close to reality) are also depicted. In the case that the minimum available photon energy is limited to 3.05 eV, the corresponding Fowler fit yields χ_{fit} = 2.63 ± 0.02 eV, as depicted in Fig. 4(a) with the red shaded area indicating the fitting range 7. This fit also describes the progression of the photocurrents in the respective range very well and is thus easily misleading in the absence of lower irradiation frequencies. As already mentioned, the Fowler T = 0 K approximation [Eq. (7)] is also routinely applied by many authors for the work function evaluation. Therefore, the respective evaluations are demonstrated in Fig. 4(b) for the sake of completeness, where the x-intercept of a linear least-squares regression of the square root of the photocurrents yields the work function (also called linearized Fowler plots). The results of the two methods are compared in Fig. 4(c) and show a good agreement in the order of $k_B T$, in agreement with the statements of Ref. 10.

By the extension of irradiation frequencies, it is now shown that the photoelectric yield progression can differ significantly from the Fowler prediction for photon energies $\gg \chi$. Thus, an insufficient lower limit of the available photon energies results in the evaluation of an overestimated work function, which is not necessarily apparent from the performed Fowler fit. In the case of using the restricted filter set, an overestimation of 0.7 eV with $\varepsilon_{ph,min} - \chi \approx 1.1$ eV is given, and hence, a severe underestimation of the given work function dynamics would be the result. One reason behind the failure of the Fowler theory for $h\nu \gg \chi$ is the fact that the Fowler fit function is derived with near threshold approximations (see Sec. II A) and is thus only accurate in a limited range above the work function (typically 0.5–1.0 eV). The near threshold approximations lead to an underestimation of the photocurrents for photon energies far above the work function, which becomes more pronounced the lower the Fermi energy is.[13] Furthermore, photon frequency dependent coefficients such as the reflectance of the surface or the transition probability of electrons through the surface potential barrier and factors such as electronic band structures and limitations of the free electron model are generally not considered in the Fowler theory. Such factors can, however, strongly influence the frequency dependent photoelectric quantum efficiency of the surface.[2,31] Since the photocurrent from the lowest photon energy mainly determines the threshold of the Fowler fit, a sufficient amount of available photon energies with a narrow spectral bandwidth is indispensable.

An indication of overestimated work functions might be given by considering the near threshold approximations that are performed in Sec. II A in order to derive the expression for the Fowler fit [Eq. (2) $\xrightarrow{\text{approx.}}$ Eq. (3) $\xrightarrow{\text{approx.}}$ Eq. (4)]. The higher the photon energies are above the threshold, these approximations induce an error that gets more pronounced. As described in detail in Ref. 13, it is for a certain work function and constant Fermi energy

$$I_{ph}^{\text{Eq. (4)}}(\varepsilon_{ph}) \le I_{ph}(\varepsilon_{ph}) \le I_{ph}^{\text{Eq. (3)}}(\varepsilon_{ph}, \varepsilon_F), \tag{9}$$

with the differences being larger for smaller ε_F. Here, $I_{ph}(\varepsilon_{ph})$ denotes the actually measured photocurrent for a particular photon energy and $I_{ph}^{\text{Eq. }(x)}$ represents the theoretical photocurrent based on the respective equation from the Fowler theory. We now consider the scenario of the decreasing surface work function during the caesiation process presented in Fig. 3 and the case that 3.05 eV is the lowest available irradiation photon energy for the work function determination, i.e., the application of the restricted filter set. Then, state "0" is defined when the work function $\chi_0 \approx 3$ eV is reached, i.e., when a photocurrent for this photon energy is detected for the first time (at t = 0.75 h in Fig. 3), and hence, the five applied photon energies for the Fowler evaluation are as close as possible to the expected real work function. The theoretical photocurrents obtained for ε_{ph} = 3.05 eV and $\chi \lesssim 3$ eV can be subsequently calculated via[13]

$$I_{ph}^{\text{Eq. (4)}}(3.05\,\text{eV}, \chi) = I_{ph,0}(3.05\,\text{eV}) \left(\frac{T}{T_0}\right)^2 \frac{f(\chi, T)}{f(\chi_0, T_0)} \tag{10}$$

and

$$I_{ph}^{\text{Eq. (3)}}(3.05\,\text{eV}, \chi, \varepsilon_F) = \sqrt{\frac{\varepsilon_{F,0} + \chi_0 - 3.05\,\text{eV}}{\varepsilon_F + \chi - 3.05\,\text{eV}}}\, I_{ph}^{\text{Eq. (4)}}. \tag{11}$$

In Fig. 5, $I_{ph}^{\text{Eq. (4)}}$ and $I_{ph}^{\text{Eq. (3)}}$ are plotted according to Eqs. (10) and (11), respectively ($T = T_0$ = 306 K). Since in the present case the evolution of the Fermi energy is unknown, physically reasonable limits are used for the calculation of $I_{ph}^{\text{Eq. (3)}}$: $\varepsilon_{F,0} = \varepsilon_{F,Mo}$ = 6.77 eV[32] and $\varepsilon_F = \varepsilon_{F,Cs}$ = 1.59 eV.[30] The region in which according to Eq. (9) the actually measured photocurrent $I_{ph}(3.05\,\text{eV})$ for $\chi \lesssim 3$ eV should lie is then given by the gray shaded area. This is confirmed by the measured values of $I_{ph}(3.05\,\text{eV})$ that are plotted against the work function χ_{ext} evaluated with the extended filter set. The plot of $I_{ph}(3.05\,\text{eV})$ against the work function χ_{restr} evaluated with the restricted filter set shows, however, an increasing deviation from the gray shaded area for $\chi_{restr} < 2.86$ eV. At the same time, the fitting constant A of the Fowler fit increases, which indicates an erroneous work function evaluation[13] and which is not the case when using the extended filter set. The correction of the work functions ($\chi_{restr} \rightarrow \chi_{corr}$) is now illustrated by the green arrows: χ_{restr} is shifted to lower values until the condition $I_{ph}^{\text{Eq. (3)}}(\chi) = I_{ph}(3.05\,\text{eV})(\chi_{corr})$ is met since $I_{ph}^{\text{Eq. (3)}}$ constitutes the upper limit for the evolution of $I_{ph}(3.05\,\text{eV})$ according to the Fowler theory. The corrected work functions are plotted in Fig. 3, and for the case of χ_{restr} = 2.63 eV for instance (evaluation see Fig. 4), the correction method yields χ_{corr} = 2.07 eV, which is only 0.12 eV larger than the value of χ_{ext}

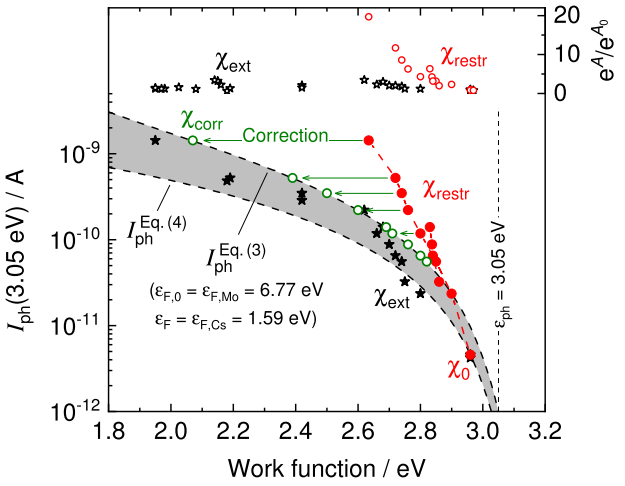

FIG. 5. Application of the correction method proposed in Ref. 13 for the work functions χ_{restr} that are evaluated with the restricted filter set: the measured photoelectric currents $I_{ph}(3.05\ eV)$ obtained from the 3.05 eV photons are plotted against χ_{restr} and are compared with the prediction of the Fowler theory using Eq. (10) for $I_{ph}^{Eq.\,(4)}$ and Eq. (11) for $I_{ph}^{Eq.\,(3)}$. The corresponding corrections of χ_{restr} are illustrated. For the sake of comparison, $I_{ph}(3.05\ eV)$ is also plotted against the work function evaluated with the extended filter set χ_{ext}. In the top part of the diagram, the evolution of a relative representation of the Fowler fit parameter A from the evaluations of χ_{restr} and χ_{ext} is depicted.

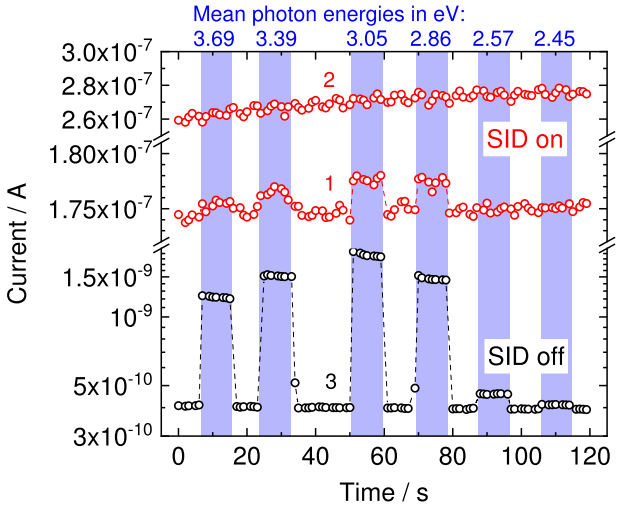

FIG. 6. Exemplary photocurrent measurements during a caesiation process shortly after the oven SID is activated (1), after some time when the SID is running (2), and immediately after the SID is switched off (3). The bluish shaded areas indicate the periods of photon irradiation with energies between 3.69 and 2.45 eV.

that is expected to be close to reality since all conditions of the Fowler theory were met. With this, the evolution of the fitting constant A as a tool for a plausibility check could be confirmed and the correction procedure was useful to come closer to the real work function. Finally, the control parameter A together with the correction procedure is a useful tool to decide on the application of lower photon energies in order to obtain absolute work function values with highest accuracy.

B. Signal-to-noise ratio

In addition to the necessity of an appropriate photon energy range and resolution for the sample irradiation, the SNR of the photoelectric measurement is an equally decisive parameter for the accuracy of the work function determination. Apart from the sensitivity of the ammeter, the SNR is mainly determined by the irradiated power density onto the surface and the level of the dark current in the electric circuit. The irradiated power density at the present setup is moderate [~ 0.1–1 mW; see Fig. 2(b)] in order to ensure that the surface is not modified by strong photon irradiation. To minimize the dark current, external noise sources (e.g., induction of electrostatic or electromagnetic interference), ground loops, tribo- and piezoelectric effects, etc., should be avoided. At the setup, unnecessary devices are switched off or are disconnected from the system during the work function measurement (e.g., optional heating of the sample holder via pulse width modulation) and the measurement itself is performed remotely, which is possible due to the automated measurement system. The active Cs evaporation into the vacuum chamber can lead to an increase of the dark current [see Fig. 3(b)], which is probably due to ionized Cs atoms and/or a higher sample leakage current caused by the work function reduction. The largest impact at the setup is given, however, by the SID diagnostic. During a similar caesiation process as shown in Fig. 3, the oven SID is activated at a point where $\chi \approx 1.9$ eV and $n_{Cs} \approx 1.5 \times 10^{15}\ m^{-3}$. With this, the dark current instantly increases by about three orders of magnitude. As a consequence, photocurrents can now only be detected for photon energies down to 2.86 eV (detection limit $\approx 2 \times 10^{-9}$ A), as is shown in Fig. 6 by the measurement labeled 1. Comparable to Fig. 4(a), the respective Fowler evaluation yields an overestimated work function of 2.59 eV. After some time, the dark current increases further and the photocurrents for ε_{ph} = 3.69–2.86 eV are then also below the detection limit (measurement labeled 2). The high dark current resulting from the oven SID can be attributed to thermionic electron emission and/or ionized Cs atoms due to the hot tungsten filaments.[22] When the oven SID is switched off again, the dark current decreases considerably and the photocurrent detection limit is $\approx 10^{-11}$ A. With this, the SNR is high enough to measure photocurrents for photon energies below 2.86 eV (measurement labeled 3) and a work function of 1.9 eV is evaluated again (measurement with an adjusted interference filter set not shown in Fig. 6). This impressively demonstrates that the noise level on which the photoelectric measurement is based must be critically taken into account when the accuracy of the determined work function value is evaluated. Measurements performed with the SID operated during the caesiation process[13,17,24,25,33,34] therefore represent only an upper limit of the actual work function.

IV. DETECTION OF ULTRA-LOW WORK FUNCTION COATINGS DURING CAESIATION UNDER MODERATE VACUUM CONDITIONS

The above-described enhancement of the photoelectric threshold sensitivity revealed work functions during caesiation in vacuum

that are substantially lower than previously measured at the ACCesS experiment.[13,17,24] In the following, the enhanced work function measurement setup is applied to monitor the caesiation process of a freshly installed polycrystalline Mo surface (SID diagnostic not in operation). One day before the conducted caesiation, a well characterized hydrogen plasma with 10 Pa gas pressure and 250 W RF power is ignited for a couple of hours in the vacuum chamber (electron temperature ~2 eV and electron density ~10^{16} m^{-3})[18] in order to remove adsorbed impurities from the Mo surface via the plasma–surface interaction and the plasma induced temperature increase close to 500 K. Since the vacuum chamber had been extensively cleaned from previous caesiations, no Cs redistribution could be detected during the plasma phase via laser absorption or optical emission spectroscopy (monitoring of 852.1 nm resonance line).

In Fig. 7(a), the temporal behavior of the surface work function during the conducted caesiation process at about room temperature is depicted. As soon as Cs vapor enters the vacuum chamber, the initial surface work function of about 4.3 eV [see the photocurrent measurement in Fig. 2(c)] is dramatically decreased. After about 45 min ($t \approx 2.2$ h), a value of slightly below 2 eV is obtained, with a neutral Cs density of ~2×10^{14} m^{-3}. The surface work function of slightly below 2 eV is kept constant as long as the Cs density in the gas phase is maintained. By further increasing the Cs evaporation rate until a neutral Cs density in the range of 10^{15} m^{-3} is reached, the photoelectric threshold decreases even further until, after some minutes, a photoelectric response is obtained in the near-infrared. This is demonstrated in Fig. 7(b), where an exemplary photocurrent monitoring with photon energies in the range of 2.04–1.45 eV is plotted, with the dark current of 4.8×10^{-10} A already subtracted. Since the absolute photocurrents for ε_{ph} = 1.85–1.45 eV are in the range of 10^{-11}–10^{-10} A, a dark current of about one order of magnitude higher would already prevent photocurrent detection, which again demonstrates the importance of a sufficient SNR. In Fig. 7(b), the respective work function evaluation via a Fowler fit is shown in the inset and yields 1.26 ± 0.01 eV. Since the control parameter A stays reasonably constant during the work function reduction down to the determined value of 1.26 eV, the trustworthiness of the Fowler evaluation can be rated as very good. Considering the finite photon energy resolution (here in the range of 0.03–0.24 eV) and the fact that photon energies below 1.45 eV are not available at the present setup, however, an absolute error of ±0.1 eV should be taken into account.

The generation of Cs coatings with an average work function of 1.25 ± 0.10 eV on a polycrystalline Mo substrate can be reliably reproduced under comparable conditions. Furthermore, the same result is obtained when the Mo substrate is replaced with a stainless steel substrate. In Fig. 8, different caesiation processes comparable to Fig. 7 are compiled for Mo and stainless steel by plotting the measured work function as a function of the applied neutral Cs flux. Since during the initial ramp-up phase of the Cs evaporation a rapid decrease of the work function on the minute scale is given, the error in the determined work function is very likely to be larger than ±0.1 eV due to the necessity of a continuous adjustment of the interference filter set and the 2 min needed for one work function measurement. Therefore, a more pronounced scattering is given in the temporal correlation of the Cs flux and the work function for $\chi \gtrsim 2.1$ eV than for $\chi \lesssim 2.1$ eV. For Cs fluxes in the range of

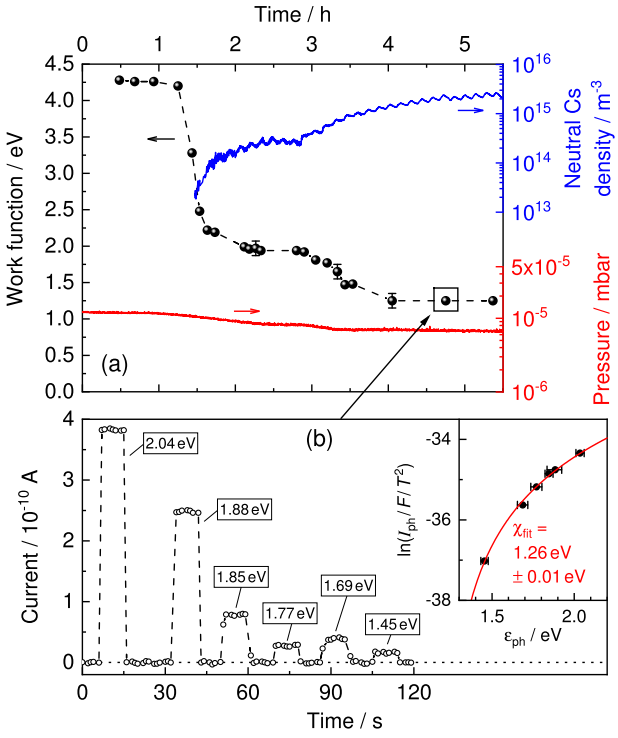

FIG. 7. Caesiation of a Mo surface under moderate vacuum conditions at about room temperature. In (a), the evolution of the photoelectric work function is plotted together with the monitored neutral Cs density and the vacuum base pressure. In (b), an exemplary photocurrent measurement for mean photon energies in the range of 2.04–1.45 eV is shown (dark current already subtracted), with the respective work function evaluation via a Fowler fit depicted in the inset (substrate temperature = 304 K).

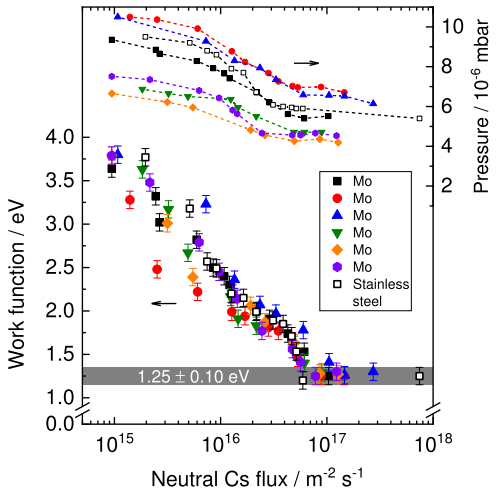

FIG. 8. Surface work function vs neutral Cs flux measured during various caesiation processes (cf. Fig. 7) of Mo and stainless steel substrates. The respective background pressures in the vacuum vessel are additionally plotted.

$\sim 10^{17}$ m^{-2} s^{-1} ($n_{Cs} \sim 1.5 \times 10^{15}$ m^{-3}), the ultra-low surface work function is achieved each time, with a background pressure of some 10^{-6} mbar. It is observed that such a threshold Cs flux is needed and cannot be compensated by increasing the Cs fluence with a lower Cs density instead (not shown here). When the Cs flux is increased close to 10^{18} m^{-2} s^{-1}, the determined work function by the Fowler method stays constant within the error bars. However, the photoelectric yield in the near-infrared increases further, and thus, the threshold of 1.25 eV might be an upper limit here. Photon energies below 1.45 eV would be needed in this case to assess the photoelectric threshold more accurately.

The generated work functions are far below the work function of bulk Cs, which is about 1.95–2.14 eV.[29,30] It is well known that work functions below the Cs bulk value can be produced via Cs coatings on metallic substrates in the (sub-)monolayer regime, which has been extensively investigated under ultra-high vacuum (UHV) conditions.[20,28,35,36] Minimum work functions for various metals, such as Cu, Ni, or W, are in the range of 1.4–1.8 eV for optimal Cs coverages, and for Mo and stainless steel, minimum work function values of 1.54–1.61 and 1.52 eV are reported, respectively.[28,35,36] Apart from the fact that no UHV conditions are given at ACCesS, a (sub-)monolayer regime as an explanation for the measured work function of 1.25 eV can, however, be excluded due to the following reasons: first, the measured work function is even lower than the reported work function minima for low Cs coverages. Second, the work function does not increase by increasing the Cs fluence. In the present case, the ultra-low work function can be maintained for several hours if the respective Cs flux is sustained. Third, a color change of the surface is visible by the eye after some time during the caesiation process, which must be due to the growth of a thick adlayer. Hence, the presence of a hydrogenated substrate, which is likely to be the case due to the hydrogen plasma treatment one day before the Cs deposition and which was found to decrease the work function minimum further in the Cs (sub-) monolayer regime,[37] is also not likely to be relevant here. Instead, it is suggested that the caesiation process under the given vacuum conditions leads to the growth of an oxidized Cs multilayer on the metal substrates and that the ultra-low work function is thus a bulk effect. It is well known that the coadsorption of Cs with electronegative species can lead to work functions that are lower than what is possible with pure Cs adsorption[36–40] and that thick overlayers with work functions down to 1.0 eV can be attained by the formation of Cs–O compounds.[41–44] In particular, the Cs oxide Cs_2O is usually proposed to provide an ultra-low work function,[41,45,46] but the mixture of Cs with other compounds such as Cs suboxides or peroxides might play a role.[42,47–50] At the given unbaked vacuum system of ACCesS, the residual gas flux is mainly composed of water vapor (indicated by RGA measurements) and is estimated to be of the order of $\Gamma_{H_2O} \sim 10^{19}$ m^{-2} s^{-1}. Thus, considerable codeposition of Cs and H_2O inevitably takes place. Interactions of the evaporated Cs with the residual gases during the caesiation process are obvious due to the decreasing background pressure by a factor of 1.5–1.8 (see Figs. 7 and 8) and are known as the Cs getter effect, i.e., the removal of residual gases due to physisorption and chemisorption. In the RGA monitoring, this effect is visible by a reduction of the H_2O signal (strong hygroscopic characteristic of Cs). Based on the measurements shown in Fig. 8, the surface work function of 1.25 eV is reached with an estimated flux ratio of the order of $\Gamma_{Cs}/\Gamma_{H_2O} \sim 0.01$. It is suggested that the coadsorption of the alkali metal with residual H_2O strongly promotes the partial and/or full dissociation of H_2O molecules on the metal surface[51–55] and consequently leads to the formation of a thick film of Cs–O(–H) compounds that provides the ultra-low surface work function. Interestingly, a good agreement is given with the reported work function of 1.22 eV in Ref. 41, which was obtained by exposing a Ag substrate alternately to Cs and H_2O in an UHV environment. To the best of the authors' knowledge, however, no measurements of the formation of a stable ultra-low Cs work function in an unbaked vacuum chamber with a base pressure of 10^{-6}–10^{-5} mbar are reported so far.

At the present setup, work functions of 2 eV and below can be kept constant only if the respective Cs flux is maintained. When a work function of 1.25 eV is reached and the Cs evaporation is subsequently shut down, a rapid degradation occurs due to the residual gas flux onto the surface: ≈2 eV is measured after about 15 min and 2.75 eV the next day. Furthermore, it should be pointed out that depending on the history of the substrate (e.g., impurity gas adsorptions or plasma exposures), re-caesiations typically lead to lower quantum efficiencies and higher surface work functions even if similar Cs densities and fluences compared to the first caesiation are applied, as can be seen for instance when comparing Fig. 7 with Fig. 3. The interaction of Cs with impurities is thus very complex, and *in situ*/*operando* surface analysis techniques are needed for a better understanding of the evolved surface composition and compounds.

V. CONCLUSIONS

The application of the Fowler theory is a well-known method for the photoelectric determination of surface work functions in vacuum. In this work, an easy-to-use setup equipped with an automated data acquisition and analysis system was used to analyze the work function evaluation of metal surfaces exposed to Cs vapor. The irradiation with photon energies from the UV to the near-infrared region is provided by a broadband emitting light source in combination with interference filters. Dedicated measurements demonstrated that a poor threshold sensitivity, which can be the result of a high dark current and/or insufficiently low available photon energies, can lead to severe errors of the evaluated work function due to the restriction of photoelectric yield data to photon energies too far away from the threshold. In the presented case of caesiated surfaces, an overestimation is the result, which increases the further the lowest irradiated photon energy is away from the threshold. The optimization of the photoelectric threshold sensitivity is thus of utmost importance to accurately access the photoelectric yield in the region close to the work function ($\lesssim 1$ eV), in which the Fowler theory can be reliably applied.

The optimized work function measurement setup used in this work provides a photon energy resolution of mostly 0.1–0.3 eV in the range of 5.04–1.45 eV, a dark current of the order of 10^{-11}–10^{-10} A, and a photocurrent detection down to the pA range, which enables access to the measurement of work functions in the ultra-low region. With this, it is now unveiled that surface work functions of 1.25 ± 0.10 eV can be reproducibly generated via caesiation of metallic surfaces (polycrystalline Mo and stainless steel) in an unbaked vacuum environment of 10^{-6}–10^{-5} mbar. Considering the moderate vacuum conditions, such a low work function is

remarkable. As long as the Cs evaporation with a neutral Cs density of the order of 10^{15} m^{-3} is sustained, the work function is temporally stable. It is assumed that this is the result of Cs coadsorption with the dominant residual water molecules, resulting in the growth of an oxidized Cs multi-adlayer on the metallic substrate. Re-caesiations of degraded Cs coatings lead to lower quantum efficiencies and higher surface work functions even for comparable Cs densities and fluences. In view of negative hydrogen ion sources, which often operate under limited vacuum conditions and in which Cs is injected (e.g., large-scale sources that are developed for upcoming fusion devices, such as ITER[56,57]), the generation of work functions in the ultra-low range on the converter surface would be highly beneficial for the enhancement of the surface production of negative ions. In a next step, the influence of plasma irradiation on such surfaces will, thus, be studied with the sensitivity enhanced work function setup at ACCesS.

ACKNOWLEDGMENTS

This work has been carried out within the framework of the EUROfusion Consortium and has received funding from the Euratomresearch and Training Programme 2014-2018 and 2019-2020 under grant agreement No. 633053. The views and opinions expressed herein do not necessarily reflect those of the European Commission. This work was carried out within the framework of the EUROfusion Consortium, funded by the European Union via the Euratom Research and Training Programme (Grant Agreement Nos. 101052200 and 633053—EUROfusion). Views and opinions expressed are, however, those of the authors only and do not necessarily reflect those of the European Union or the European Commission. Neither the European Union nor the European Commission can be held responsible for them.

AUTHOR DECLARATIONS

Conflict of Interest

The authors have no conflicts to disclose.

DATA AVAILABILITY

The data that support the findings of this study are available from the corresponding author upon reasonable request.

REFERENCES

[1] R. H. Fowler, "The analysis of photoelectric sensitivity curves for clean metals at various temperatures," Phys. Rev. **38**, 45–56 (1931).
[2] C. N. Berglund and W. E. Spicer, "Photoemission studies of copper and silver: Experiment," Phys. Rev. **136**, A1044–A1064 (1964).
[3] A. J. Blodgett and W. E. Spicer, "Experimental determination of the density of states in nickel," Phys. Rev. **146**, 390–402 (1966).
[4] D. E. Eastman, "Photoelectric work functions of transition, rare-earth, and noble metals," Phys. Rev. B **2**, 1–2 (1970).
[5] M. Wada, K. H. Berkner, R. V. Pyle, and J. W. Stearns, "Photoelectric work function measurement of a cesiated metal surface and its correlation with the surface-produced H^- ion flux," J. Vac. Sci. Technol. A **1**, 981–984 (1983).
[6] M. Akbi and A. Lefort, "Work function measurements of contact materials for industrial use," J. Phys. D: Appl. Phys. **31**, 1301–1308 (1998).
[7] R. Schletti, P. Wurz, and T. Fröhlich, "Metallic work function measurement in the range 2–3.3 eV using a blue light-emitting diode source," Rev. Sci. Instrum. **71**, 499–503 (2000).
[8] K. Wong, G. Tikhonov, and V. V. Kresin, "Temperature-dependent work functions of free alkali-metal nanoparticles," Phys. Rev. B **66**, 125401 (2002).
[9] E. Czerwosz, P. Dłużewski, M. Kozłowski, R. Nowakowski, and T. Stacewicz, "Photoelectric work function determination for the nanostructural carbonaceous films," Vacuum **70**, 237–241 (2003).
[10] M. Akbi, A. Bouchou, and N. Zouache, "Effects of vacuum heat treatment on the photoelectric work function and surface morphology of multilayered silver–metal electrical contacts," Appl. Surf. Sci. **303**, 131–139 (2014).
[11] J. Hölzl and F. K. Schulte, "Work function of metals," in *Solid Surface Physics*, edited by J. Hölzl, F. K. Schulte, and H. Wagner (Springer Berlin Heidelberg, Berlin, Heidelberg, 1979), pp. 1–150.
[12] L. W. Swanson and P. R. Davis, "1. Work function measurements," in *Solid State Physics: Surfaces, Methods in Experimental Physics*, edited by R. L. Park and M. G. Lagally (Academic Press, 1985), Vol. 22, pp. 1–22.
[13] R. Friedl, "Enhancing the accuracy of the Fowler method for monitoring non-constant work functions," Rev. Sci. Instrum. **87**, 043901 (2016).
[14] A. Kahn, "Fermi level, work function and vacuum level," Mater. Horiz. **3**, 7–10 (2016).
[15] L. A. DuBridge, "A further experimental test of Fowler's theory of photoelectric emission," Phys. Rev. **39**, 108–118 (1932).
[16] L. A. DuBridge and W. W. Roehr, "Photoelectric and thermionic properties of palladium," Phys. Rev. **39**, 99–107 (1932).
[17] S. Cristofaro, R. Friedl, and U. Fantz, "Correlation of Cs flux and work function of a converter surface during long plasma exposure for negative ion sources in view of ITER," Plasma Res. Express **2**, 035009 (2020).
[18] R. Friedl and U. Fantz, "Fundamental studies on the Cs dynamics under ion source conditions," Rev. Sci. Instrum. **85**, 02B109 (2014).
[19] S. Cristofaro, M. Fröschle, A. Mimo, A. Rizzolo, M. De Muri, M. Barbisan, and U. Fantz, "Design and comparison of the Cs ovens for the test facilities ELISE and SPIDER," Rev. Sci. Instrum. **90**, 113504 (2019).
[20] H. P. Bonzel, "Alkali-metal-affected adsorption of molecules on metal surfaces," Surf. Sci. Rep. **8**, 43–125 (1988).
[21] T. Aruga and Y. Murata, "Alkali-metal adsorption on metals," Prog. Surf. Sci. **31**, 61–130 (1989).
[22] U. Fantz, R. Friedl, and M. Fröschle, "Controllable evaporation of cesium from a dispenser oven," Rev. Sci. Instrum. **83**, 123305 (2012).
[23] U. Fantz and C. Wimmer, "Optimizing the laser absorption technique for quantification of caesium densities in negative hydrogen ion sources," J. Phys. D: Appl. Phys. **44**, 335202 (2011).
[24] R. Friedl and U. Fantz, "Influence of H_2 and D_2 plasmas on the work function of caesiated materials," J. Appl. Phys. **122**, 083304 (2017).
[25] S. Cristofaro, R. Friedl, and U. Fantz, "Negative hydrogen and deuterium ion density in a low pressure plasma in front of a converter surface at different work functions," Plasma **4**, 94–107 (2021).
[26] M. Bacal and M. Wada, "Negative hydrogen ion production mechanisms," Appl. Phys. Rev. **2**, 021305 (2015).
[27] U. Fantz and J. Lettry, "Focus on sources of negatively charged ions," New J. Phys. **20**, 060201 (2018).
[28] R. G. Wilson, "Electron and ion emission from polycrystalline surfaces of Nb, Mo, Ta, W, Re, Os, and Ir in cesium vapor," J. Appl. Phys. **37**, 4125–4131 (1966).
[29] H. B. Michaelson, "The work function of the elements and its periodicity," J. Appl. Phys. **48**, 4729–4733 (1977).
[30] *CRC Handbook of Chemistry and Physics*, edited by W. M. Haynes (CRC Press, 2016).
[31] L. A. DuBridge, "Electron emission from metal surfaces," Am. J. Phys. **16**, 191–198 (1948).
[32] I. Petroff and C. R. Viswanathan, "Calculation of density of states in W, Ta, and Mo," Nat. Bur. Stand. (U. S.), Spec. Publ. **323**, 53–56 (1971).
[33] R. Friedl and U. Fantz, "Temperature dependence of the work function of caesiated materials under ion source conditions," AIP Conf. Proc. **1655**, 020004 (2015).
[34] S. Cristofaro, R. Friedl, and U. Fantz, "Simultaneous measurements of work function and H^- density including caesiation of a converter surface," AIP Conf. Proc. **1869**, 030036 (2017).

[35]R. G. Wilson, "Electron and ion emission from polycrystalline surfaces of Be, Ti, Cr, Ni, Cu, Pt, and type-304 stainless steel in cesium vapor," J. Appl. Phys. **37**, 3161–3169 (1966).
[36]L. W. Swanson and R. W. Strayer, "Field-electron-microscopy studies of cesium layers on various refractory metals: Work function change," J. Chem. Phys. **48**, 2421–2442 (1968).
[37]C. A. Papageorgopoulos and J. M. Chen, "Coadsorption of electropositive and electronegative elements: I. Cs and H_2 on W(100)," Surf. Sci. **39**, 283–312 (1973).
[38]C. A. Papageorgopoulos and J. M. Chen, "Coadsorption of electropositive and electronegative elements: II. Cs and O_2 on W (100)," Surf. Sci. **39**, 313–332 (1973).
[39]J.-L. Desplat and C. A. Papageorgopoulos, "Interaction of cesium and oxygen on W(110): I. Cesium adsorption on oxygenated and oxidized W(110)," Surf. Sci. **92**, 97–118 (1980).
[40]C. A. Papageorgopoulos, "Studies of separate adsorption and coadsorption of Cs and O_2 on Cu(100)," Phys. Rev. B **25**, 3740–3749 (1982).
[41]J. J. Uebbing and L. W. James, "Behavior of cesium oxide as a low work-function coating," J. Appl. Phys. **41**, 4505–4516 (1970).
[42]T. R. Briere and A. H. Sommer, "Low-work-function surfaces produced by cesium carbonate decomposition," J. Appl. Phys. **48**, 3547–3550 (1977).
[43]L. R. Danielson, "Coadsorption of cesium and oxygen on iridium and lanthanum hexaboride," J. Appl. Phys. **52**, 300–304 (1981).
[44]S. T. Melnychuk and M. Seidl, "Reflection of hydrogen atoms from alkali and alkaline earth oxide surfaces," J. Vac. Sci. Technol. A **9**, 1650–1656 (1991).
[45]J. E. Davey, "Thermionic and semiconducting properties of [Ag]-Cs_2O, Ag, Cs," J. Appl. Phys. **28**, 1031–1034 (1957).
[46]J.-L. Desplat, "Work function of Mo(110) in mixed cesium and cesium monoxide vapors," J. Appl. Phys. **54**, 5494–5497 (1983).
[47]P. E. Gregory, P. Chye, H. Sunami, and W. E. Spicer, "The oxidation of Cs–uv photoemission studies," J. Appl. Phys. **46**, 3525–3529 (1975).
[48]G. Ebbinghaus and A. Simon, "Electronic structure of Rb, Cs and some of their metallic oxides studied by photoelectron spectroscopy," Chem. Phys. **43**, 117–133 (1979).
[49]S.-J. Yang and C. W. Bates, "The role of cesium suboxides in low-work-function surface layers studied by x-ray photoelectron spectroscopy: Ag–O–Cs," Appl. Phys. Lett. **36**, 675–677 (1980).
[50]B. Woratschek, W. Sesselmann, J. Küppers, G. Ertl, and H. Haberland, "The interaction of cesium with oxygen," J. Chem. Phys. **86**, 2411–2422 (1987).
[51]P. A. Thiel and T. E. Madey, "The interaction of water with solid surfaces: Fundamental aspects," Surf. Sci. Rep. **7**, 211–385 (1987).
[52]G. Pirug, C. Ritke, and H. P. Bonzel, "Adsorption of H_2O on Ru(001): II. Effect of coadsorbed alkali metals (Na, K, Cs)," Surf. Sci. **257**, 50–62 (1991).
[53]H. Shi and K. Jacobi, "Reaction between H_2O and Cs on the Ru(001) surface," Surf. Sci. **317**, 45–57 (1994).
[54]M. A. Henderson, "The interaction of water with solid surfaces: Fundamental aspects revisited," Surf. Sci. Rep. **46**, 1–308 (2002).
[55]D. Vlachos, E. Giotopoulou, and M. Kamaratos, "Adsorption of water on a cesium covered $SrTiO_3$ (100) surface," Proc. NAP **3**, 01NTF15 (2014).
[56]R. S. Hemsworth, D. Boilson, P. Blatchford, M. D. Palma, G. Chitarin, H. P. L. de Esch, F. Geli, M. Dremel, J. Graceffa, D. Marcuzzi, G. Serianni, D. Shah, M. Singh, M. Urbani, and P. Zaccaria, "Overview of the design of the ITER heating neutral beam injectors," New J. Phys. **19**, 025005 (2017).
[57]U. Fantz, S. Briefi, A. Heiler, C. Wimmer, and D. Wünderlich, "Negative hydrogen ion sources for fusion: From plasma generation to beam properties," Front. Phys. **9**, 709651 (2021).